

Hyperspectral Image Super-Resolution with Spectral Mixup and Heterogeneous Datasets

Ke Li¹ Dengxin Dai¹ Ender Konukoglu¹ Luc Van Gool^{1,2}

¹CVL, ETH Zurich, ²PSI, KU Leuven

{ke.li, dai, ender.konukoglu, vangool}@vision.ee.ethz.ch

Abstract

This work studies Hyperspectral image (HSI) super-resolution (SR). HSI SR is characterized by high-dimensional data and a limited amount of training examples. This exacerbates the undesirable behaviors of neural networks such as memorization and sensitivity to out-of-distribution samples. This work addresses these issues with three contributions. First, we observe that HSI SR and RGB image SR are correlated and develop a novel multi-tasking network to train them jointly so that the auxiliary task RGB image SR can provide additional supervision. Second, we propose a simple, yet effective data augmentation routine, termed Spectral Mixup, to construct effective virtual training samples to enlarge the training set. Finally, we extend the network to a semi-supervised setting so that it can learn from datasets containing only low-resolution HSIs. With these contributions, our method is able to learn from heterogeneous datasets and lift the requirement for having a large amount of HD HSI training samples. Extensive experiments on four standard datasets show that our method outperforms existing methods significantly and underpin the relevance of our contributions. Code has been made available at <https://github.com/kli8996/HSISR>.

1. Introduction

Hyperspectral imaging acquires images across many intervals of the electromagnetic spectrum. It has been applied to numerous areas such as medical diagnosis [37], food quality and safety control [22], remote sensing [21] and object detection [39]. All these applications benefit from analyzing the spectral information coming with HSIs. One obstacle in the way of further unleashing this potential is data acquisition. Acquiring HSIs of high spatial and high spectral resolution at a high frame rate is still a grand challenge. There is still no camera to achieve these three goals at the same time. Cameras for a compromise setting – high spectral but low spatial resolution – are quite common by

now, though still expensive. As a result, increasing efforts have been made to advance HSI super-resolution (SR).

While numerous deep learning methods have been developed for improving the resolution of RGB images (RGBIs), the topic of HSI SR has received little attention. One of the main reasons is the lack of large-scale HSI datasets for high-resolution (HR) HSIs. As known, supervised deep learning methods need an enormous amount of training data. This situation, unfortunately, will not be improved in the foreseeable future due to the challenges hyperspectral imaging faces. In this work, we choose a different route and propose to learn from multiple heterogeneous datasets and also from virtual examples. We find that while it is difficult to collect HR HSIs, it is relatively easy to collect only LR HSIs and it is very easy to collect HR RGB images. It is thus appealing to have a HSI SR method which can learn from these heterogeneous sources. Our method is designed for this aim.

Although the data distribution is not the same between RGBIs and HSIs, the two SR tasks do share some common goals in integrating information from neighboring spatial regions and neighboring spectral bands during the learning. We embrace this observation and formulate both tasks into the same learning framework such that the parameter distribution induced by the RGBI SR task can serve as an effective regularization for our HSI SR task. The challenge lies in the difference in spectral band numbers, e.g. three in RGBIs vs. e.g. 31 or 128 in HSIs. To tackle this and to reduce the computational complexity, we propose a universal group convolutional neural network that can accommodate different spectral groups.

We further propose a data augmentation routine, termed *Spectral Mixup*, to create effective ‘virtual’ training examples. Data augmentation is a strategy to create virtual samples by modifying the original samples. Data augmentation is known to increase the generalizability of learning methods. Common methods for classification tasks include reflections, rotations, cropping, and color jittering. They assume that examples obtained by those operations share the same class with the original example and that can hardly be applied to our regression task. In this work, we propose

Spectral Mixup to create virtual samples using convex combinations of spectral bands of the same image for our task HSI SR. *Spectral Mixup* favors functions that preserve simple linear behavior in-between spectral bands and greatly avoids data over-fitting.

While the aforementioned contributions can yield state-of-the-art performance already, we extend the method further to learn from unlabeled datasets as well. Semi-supervised learning (SSL) exploits unlabeled data to reduce over-fitting to the limited amount of labeled data [15, 31, 45, 48, 24]. While good progress has been achieved, the strategies are mainly designed for recognition tasks. Their applicability to a low-level dense regression task such as HSI SR has yet to be verified. In this work, we again leverage the success of RGBI SR and propose a cross-model consistency that favors functions giving consistent outputs between super-resolved RGBIs and super-resolved HSIs. Basically, we convert LR HSIs into LR RGB images and pass those through the RGBI SR network. In the meanwhile, we pass the LR HSIs through our HSI SR network to get the super-resolved HSIs and convert them to RGBIs with a standard camera response function. We enforce the consistency between the two versions of super-resolved RGBIs. This way, supervision is transferred from the better-trained RGB SR network to our HSI SR network via a second route.

To summarize, this work makes three contributions: 1) a multi-tasking HSI SR method to learn together with an auxiliary RGBI SR task; 2) a simple, yet effective data augmentation method *Spectral Mixup*; and 3) A SSL method to learn also from ‘unlabeled’ LR HSIs. With these contributions, our method sets the new state of the art.

2. Related Work

Hyperspectral Image Super-Resolution. HSI SR can be grouped into three categories according to their settings: 1) HSI SR from only RGBIs; 2) Single HSI SR from LR HSIs; and 3) HSI SR from both HR RGBIs and LR HSIs of the same scene. Our method belongs to the second group.

HSR SR from only RGBIs is a highly ill-posed problem. However, it has gained great traction in recent years due to its simple setup and the well-organized workshop challenges [8]. Similar to other computer vision topics, the trend has shifted from ‘conventional’ methods such as radial basis functions [40] and sparse coding [7] to deep neural networks [20, 44, 8]. This trend highlights the need for bigger training datasets.

Single image SR aims to model the relationship between the LR images and HR ones by learning from a collection of examples consisting of pairs of HR images and LR images. Single RGBI SR has achieved remarkable results in the last years. Since the first work of using neural networks for the task [17], progress has been made in making networks deeper and the connections denser [27, 59], using feature

pyramids [30], employing GAN losses [33], and modeling real-world degradation effects [23]. As to single HSI SR, there has been great early work [3, 60] as well. However, that is also surpassed by deep learning methods. For instance, Yuan *et al.* [54] trained a single-band SR method on natural image datasets, and applied it to HSIs in a band-wise manner to explore spatial information. The spectral information is explored via matrix factorization afterwards. In order to explore both spatial and spectral correlation at the same time, methods based on 3D Convolutional Networks [38, 34] have been developed. Although 3D CNNs sound like a perfect solution, the computational complexity is very high. To alleviate this, Grouped Convolutions (GCs) with shared parameters have been recently used in [35, 26]. The backbone network of our method is also based on GCs.

Fusion-based methods use HR RGBIs of the same scene as references to improve the spatial resolution of the LR HSIs [11, 51]. This stream of methods have received more research attention than the former two. Many learning techniques have been applied to this data fusion task including Bayesian inference [5, 6, 58], matrix factorization [32, 16], sparse representation [4, 18], and deep neural networks [41, 49]. The common goal of these methods is to learn to propagate the detailed information in the HR RGBIs to the target HSIs and fuse them with the fundamental spectral information from LR HSIs. Despite the plethora of fusion algorithms developed, they all assume that the LR HSIs and the HR RGBIs are very well co-registered [26]. This data registration is a challenge on its own and registration errors will lead to degraded SR results [13, 61].

Learning with Auxiliary Tasks. It is quite a common practice to borrow additional supervision from related auxiliary tasks, when there is insufficient data to learn a task. The common strategy is to learn all the tasks together so that the auxiliary tasks can regularize the optimization. There are normally two assumptions: (1) we only care about the performance of the main task and (2) the supervision for the auxiliary tasks is easier to obtain than that of the main task. Previous work has employed various kinds of self-supervised methods as auxiliary tasks for the main supervised task in a semi-supervised setting [29, 10, 42]. For instance, generative approaches have been explored in [29] and predicting the orientation of image patches is used in [10]. Another related setting is multi-task learning (MTL) [46]. In MTL, the goal is to reach high performance on multiple tasks simultaneously, so all tasks are main tasks and all tasks are auxiliary tasks. While the goal is different, many strategies in MTL such as parameter sharing [9], task consistency [56], and loss balance [14] are useful for learning with auxiliary tasks.

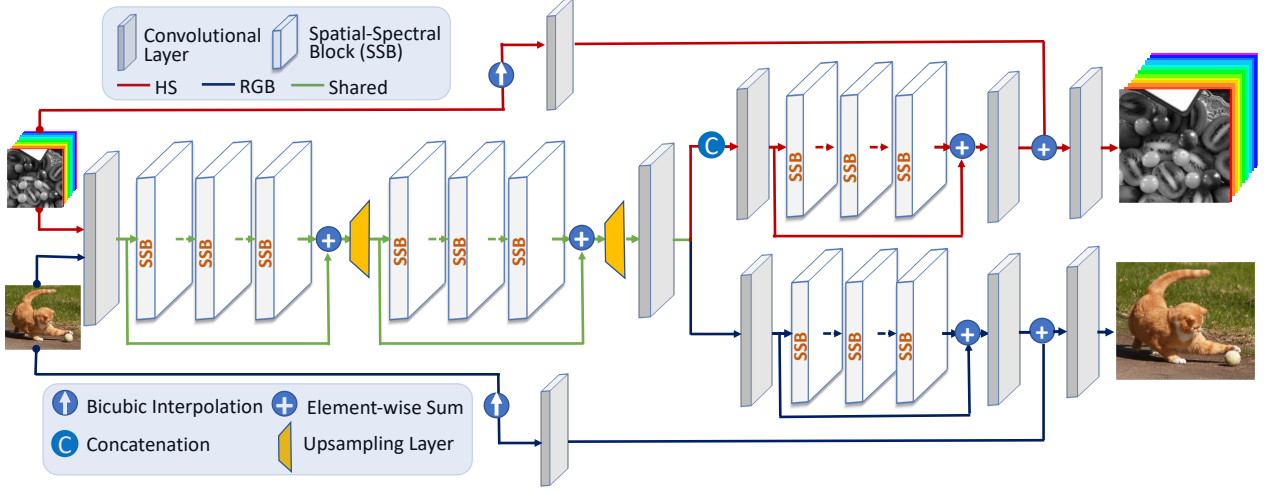


Figure 1: The architecture of our network consisting of a shared encoder and two specific decoders for the two SR tasks.

3. Approach

HSIs provide tens of narrow bands, so processing all the bands together is time-consuming and requires very large datasets in order to avoid over-fitting. In this work, we follow [26] and use a grouping strategy to divide input HSIs into overlapping groups of bands. This way, the spectral correlation among neighboring bands can be effectively exploited without increasing the parameters of the model. Another major advantage of using a grouping strategy is that it offers the possibility to train our auxiliary task RGBI SR along with our main task HSI SR within the same network. Without using the grouping strategy, the difference in the number of bands is very large between the two tasks. In this work, we assume that the relationships between low/high-resolution HSIs and low/high-resolution RGBIs are correlated, so they should be trained together so that RGBI SR can provide additional supervision for HSI SR. This way, the HSI SR method can enjoy training samples of a much more diverse set of scenes especially those that cannot be captured well by current hyperspectral imaging devices such as moving objects.

3.1. HSI SR with an Auxiliary RGBI SR Task

Given two SR tasks \mathcal{T}_{HS} and \mathcal{T}_{RGB} , we aim to help improve the learning of a model for \mathcal{T}_{HS} by using the knowledge contained in \mathcal{T}_{RGB} . In the supervised setting, each task is accompanied by a training dataset consisting of N training samples, i.e., $\mathcal{D}_{\text{HS}} = \{\mathbf{x}_{\text{HS}}^i, \mathbf{X}_{\text{HS}}^i\}_{i=1}^{N_{\text{HS}}}$ and $\mathcal{D}_{\text{RGB}} = \{\mathbf{x}_{\text{RGB}}^i, \mathbf{X}_{\text{RGB}}^i\}_{i=1}^{N_{\text{RGB}}}$, where $\mathbf{x}_{\text{HS}} \in \mathbb{R}^{h_1 \times w_1 \times C}$, $\mathbf{X}_{\text{HS}} \in \mathbb{R}^{H_1 \times W_1 \times C}$, $\mathbf{x}_{\text{RGB}} \in \mathbb{R}^{h_2 \times w_2 \times Z}$, and $\mathbf{X}_{\text{RGB}} \in \mathbb{R}^{H_2 \times W_2 \times Z}$. We denote low-resolution (LR) images by \mathbf{x} , high-resolution (HR) images by \mathbf{X} , the number of bands of HSIs by C , the number of bands in RGB images by Z (3

here), and the size of the images by h, w, H and W . Given a scaling factor τ , we have $H_i = \tau h_i$ and $W_i = \tau w_i$ for both tasks.

The goal is to train a neural network Φ_{HS} to predict the HR HSI for a given LR HSI: $\mathbf{X}_{\text{HS}} = \Phi_{\text{HS}}(\mathbf{x}_{\text{HS}})$. Different from previous methods, which have a single network for the whole task, our method consists of three blocks: an encoder which is shared by the two SR tasks, and two task-specific decoders to output the final outputs. More specifically, $\Phi_{\text{HS}} = (\Phi^{\text{En}}, \Phi_{\text{HS}}^{\text{De}})$ and $\Phi_{\text{RGB}} = (\Phi^{\text{En}}, \Phi_{\text{RGB}}^{\text{De}})$. The general architecture is shown in Fig 1.

In order to share the same encoder between the two SR tasks, we divide the C input channels of \mathbf{x}_{HS} into groups of M bands. For HSI SR, the encoder network Φ^{En} takes M channels as input and generates M channels as output. The outputs of all the groups of \mathbf{x}_{HS} are then concatenated according to their original spectral band position to assemble a new HSI $\tilde{\mathbf{X}}_{\text{HS}} \in \mathbb{R}^{H_1 \times W_1 \times C}$. The neighboring groups of \mathbf{x}_{HS} can have overlaps and we average the results of the overlapping areas when assembling $\tilde{\mathbf{X}}_{\text{HS}}$. There are two up-sampling layers to upscale the size of the input to the desired size in a progressive manner. This progressive upsampling has proven useful for both RGBI SR [30] and HSI SR [26]. The reconstructed $\tilde{\mathbf{X}}_{\text{HS}}$ is then fed into the decoder network $\Phi_{\text{HS}}^{\text{De}}$ as a whole to generate the final output $\hat{\mathbf{X}}_{\text{HS}}$, which is then compared to the ground truth \mathbf{X}_{HS} to compute the loss. $\Phi_{\text{HS}}^{\text{De}}$ takes all the bands directly to learn long-range spectral correlations beyond individual groups to refine the results.

For RGBI SR, we first increase the number of bands of \mathbf{x}_{RGB} from Z to M via a simple spectral interpolation which will be explained in Sec. 3.1.1. The interpolated M -band image is then passed through the encoder Φ^{En} to obtain a new M -band RGB image $\tilde{\mathbf{X}}_{\text{RGB}} \in \mathbb{R}^{H_2 \times W_2 \times M}$ of the desired resolution. Because the decoder is shared by two

tasks, $\bar{\mathbf{X}}_{\text{RGB}}$ is also needed to be fed to its own task-specific decoder network $\Phi_{\text{RGB}}^{\text{De}}$ for further refinement. The final output $\hat{\mathbf{X}}_{\text{RGB}}$ from $\Phi_{\text{RGB}}^{\text{De}}$ is then compared to the ground-truth image \mathbf{X}_{RGB} .

In order to have a modular design, the three sub-networks have the same basic architecture. They are all composed of a sequence of Spatial-Spectral Block (SSB) modules. The SBB module was proposed in [26] as a basic building block for their HSI SR network. Each SBB has a Spatial Residual Module and a Spectral Attention Residual Module. Two Convolutional layers (the first one followed by a ReLU layer) with 3x3 filters are used in the Spatial Residual Module to capture spatial correlations. Two Convolutional layers (the first one again followed by a ReLU layer) with 1x1 filters are used in the Spectral Attention Residual Module to capture spectral correlations. Please refer to Fig.2 in [26] for more details of the SBB module. We construct the whole network with standard Convolutional Layers, SBBs, Upsampling Layers and Concatenation Operations. There are also skip connections at multiple scales to facilitate the information flow. The input LR images are also scaled to the desired size via Bicubic Interpolation and fused with the network output for residual learning. The complete network is shown in Fig. 1. We employ the PixelShuffle [43] operator for the upsampling layer. Given a scaling factor τ , the first upsampling layer upscales the features $\tau/2$ times and the second one handles the remaining $\times 2$ factor. The internal features of all SBB modules are limited to 256 in this work. The filter size of all Convolutional Layers, except for those in the Spectral Attention Residual Module of SBBs, are set to 3×3 .

3.1.1 Spectral Interpolation of RGB Images

The task is to increase the number of band from Z to M for RGB images. For instance, we have $Z = 3$ and $M = 8$ in this work. Because the generated M -band images will be used to train the SR network for supervision transfer to HSI SR, we posit that these new images need to have certain properties. First, they should not contain artifacts. Second, the correlation between the bands of the new images should follow a distance rule in that the correlation between neighboring HSI bands should be higher than that between distant bands. For this, we propose a simple interpolation method. Given Z bands, we interpolate $K = (M - Z)/(Z - 1)$ new bands to each of the $Z - 1$ intervals between consecutive bands. For the i^{th} band $\hat{\mathbf{x}}(i)$ between the original bands z and $z + 1$, we have:

$$\hat{\mathbf{x}}(i) = (1 - \frac{i}{K+1})\mathbf{x}(z) + \frac{i}{K+1}\mathbf{x}(z+1). \quad (1)$$

Note that if K is not an integer, we use $\lceil K \rceil$ for the first interval and $\lfloor K \rfloor$ for the second one.

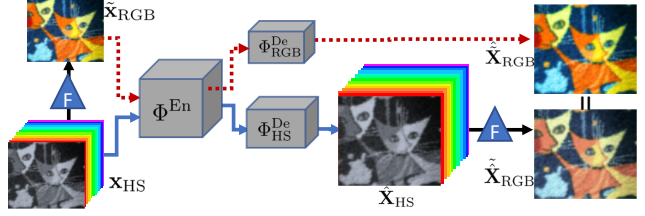


Figure 2: The pipeline of our semi-supervised learning.

3.2. Spectral Mixup

Data augmentation is a strategy to create virtual samples by alternating the original samples. The recent *mixup* method [57] creates virtual examples by using convex combinations of pairs of examples and their labels. While it is very effective for high-level classification tasks, it does not offer help for low-level SR tasks [53] because the detailed image structures can be destroyed by the mixing-up of two images. These detailed structures are important for SR tasks. Taking into account of this observation, we propose a data augmentation routine *Spectral Mixup* specifically for HSI SR. It creates virtual samples and their ground truths by using convex combinations of spectral bands within self-image and within its ground-truth image, respectively.

More specifically, given \mathbf{x}_{HS} and its ground truth \mathbf{X}_{HS} , both with C channels, we generate a mixing matrix $B \in \mathbb{R}^{C \times C}$ filled with random numbers sampled from a uniform distribution on the interval $[0, 1)$. B is then row-wise normalized to make sure that the values in the projected image have the same magnitude as that of the original image. The new example and its ground truth are then created as:

$$\hat{\mathbf{x}}_{\text{HS}}^{(i,j)} = \alpha \mathbf{x}_{\text{HS}}^{(i,j)} + (1 - \alpha) B \mathbf{x}_{\text{HS}}^{(i,j)}, \quad (2)$$

$$\hat{\mathbf{X}}_{\text{HS}}^{(i,j)} = \alpha \mathbf{X}_{\text{HS}}^{(i,j)} + (1 - \alpha) B \mathbf{X}_{\text{HS}}^{(i,j)}, \quad (3)$$

where (i,j) index over all positions to get the values of pixels. The randomly projected images are fused with the original images to strike a balance between increasing variations and preserving the fidelity of real HSIs. For instance, the relationships between the bands of real HSIs should be largely kept. In this work, α is set to 0.5 and we study the influence of this parameter in Sec. 4. The implementation of *Spectral Mixup* training is very straightforward and can be done with a few lines of code. *Spectral Mixup* also introduces very little computation overhead. By applying it, more examples from the vicinity of the original example can be sampled. Learning with those new examples encourages the network to have simple linear behavior in-between spectral bands which is found very useful for HSI SR.

3.3. Semi-Supervised HSI SR

While training with auxiliary RGB SR task and *Spectral Mixup* can greatly improve the performance, there is still a

strong need to also learn with unlabeled HSIs, *i.e.* LR HSIs without HR HSIs as ground truth. This is especially true as modern snapshot HS cameras that captures LR HSIs at high frame rate are becoming more and more accessible. In the literature, there has been a diverse sets of methods developed for semi-supervised learning (SSL) based on techniques such as entropy minimization and pseudo-labels generation. However, they are mostly designed for high-level recognition tasks and can not be applied to HSI SR directly.

In this work, we propose a new SSL method specifically for HSI SR. For this purpose, we again leverage the fact that RGBI SR is a better-addressed problem, given that it has a large amount of training data and it predicts only three channels. The method works as follows: given an image \mathbf{x}_{HS} , we convert it to an RGB image $\tilde{\mathbf{x}}_{\text{RGB}}$ with the camera response function of a standard RGB camera \mathbf{f} : $\tilde{\mathbf{x}}_{\text{RGB}}^{(i,j)} = \mathbf{f} * \mathbf{x}_{\text{HS}}^{(i,j)}$, where $*$ is a convolution operation. The operation is to integrate the spectra signatures into R, G, and B channels and is widely used in the literature [19]. The response function of Canon 1D Mark 3 [25] is used in this work but other camera response functions can also be used.

The original HSI \mathbf{x}_{HS} and the converted RGB image $\tilde{\mathbf{x}}_{\text{RGB}}$ are then fed into the HSI SR network Φ_{HS} and the RGBI SR network Φ_{RGB} , respectively, to generate the super-resolved results: $\hat{\mathbf{X}}_{\text{HS}} = \Phi_{\text{HS}}(\mathbf{x}_{\text{HS}})$ and $\hat{\mathbf{X}}_{\text{RGB}} = \Phi_{\text{RGB}}(\tilde{\mathbf{x}}_{\text{RGB}})$; $\hat{\mathbf{X}}_{\text{HS}}$ is then converted to an RGB image by using the same camera response function: $\hat{\tilde{\mathbf{X}}}_{\text{RGB}}^{(i,j)} = \mathbf{f} * \hat{\mathbf{X}}_{\text{HS}}^{(i,j)}$. Finally, a consistency loss $L_{\text{ssl}}(\hat{\mathbf{X}}_{\text{RGB}}, \hat{\tilde{\mathbf{X}}}_{\text{RGB}})$ is computed between the two HR RGB results. This consistency check makes a good use of ‘unlabeled’ HSIs and ‘labeled’ RGB images. It transfers supervision from the RGB side to the HSI side. The diagram of this SSL method is shown in Fig. 2.

3.4. Loss Function

In order to capture both spatial and spectral correlation of the SR results, we follow [26] and combine the L1 loss and the spatial-spectral total variation (SSTV) loss [1]. SSTV is used to encourage smooth results in both spatial domain and spectral domain and it is defined as:

$$\mathcal{L}_{\text{SSTV}} = \frac{1}{N} \sum_{n=1}^N (||\nabla_{\text{h}} \hat{\mathbf{X}}^n||_1 + ||\nabla_{\text{w}} \hat{\mathbf{X}}^n||_1 + ||\nabla_{\text{c}} \hat{\mathbf{X}}^n||_1), \quad (4)$$

where ∇_{h} , ∇_{w} , and ∇_{c} compute gradient along the horizontal, vertical and spectral directions, resp. The loss is:

$$\mathcal{L} = \mathcal{L}_1 + \mathcal{L}_{\text{SSTV}}. \quad (5)$$

The overall loss for our SR tasks is:

$$\begin{aligned} \mathcal{L}^{\text{Total}} = & \mathcal{L}^{\text{HS}}(\mathbf{X}_{\text{HS}}, \hat{\mathbf{X}}_{\text{HS}}) + \mathcal{L}^{\text{RGB}}(\mathbf{X}_{\text{RGB}}, \hat{\mathbf{X}}_{\text{RGB}}) \\ & + \mathcal{L}^{\text{SMixup}}(\hat{\mathbf{X}}_{\text{HS}}, \hat{\tilde{\mathbf{X}}}_{\text{HS}}) + \mathcal{L}^{\text{SSL}}(\hat{\mathbf{X}}_{\text{RGB}}, \hat{\tilde{\mathbf{X}}}_{\text{RGB}}). \end{aligned} \quad (6)$$

The main loss is augmented by the three auxiliary losses which are optional but highly beneficial. A joint training with all losses together works well in principle by stacking multiple types of data samples in a single mini-batch. However, that will heavily limits the size of the training data for each loss. In this work, we adopt an alternating training strategy; that is to train with each of the four losses in turn in every iteration. In our implementation, the weights for all losses are set to 1. The contributions of different terms are balanced or controlled by altering the number of mini-batches for that loss in each iteration. The influence of these numbers are studied in Sec. 4.2.

4. Experiments

4.1. Experimental Setup

Datasets. We evaluate our method on four public datasets. The datasets considered are three nature HSI datasets: CAVE dataset [50], Harvard dataset [12], and NTIRE 2020 dataset [8], and one remote sensing HSI dataset Chikusei [52]. Images in CAVE and NTIRE 2020 dataset have 31 bands ranging from 400 nm to 700 nm at a step of 10 nm. Images in Harvard dataset contain 31 bands as well but range from 420 nm to 720 nm. The Chikusei dataset has 128 bands spanning from 363 nm to 1018 nm.

The CAVE dataset contains 32 images of 512 x 512 pixels. We use 20 images for training and 10 images for testing. We evaluated in a supervised setting and a semi-supervised setting. For our semi-supervised setting, 5 images are used as labeled images (with HR HSIs) and the remaining 15 used as unlabeled. For the Harvard dataset, there are 50 images in total. We use 40 for training and 10 for test. For the semi-supervised setting, 6 images are taken as the labeled images while the remaining 34 are taken as unlabeled images. For NTIRE 2020, there are 480 images. We use 400 images for training and 80 images for test. For the semi-supervised case, we further split the 400 images into 100 as labeled images and 300 as unlabeled images. For Chikusei, there is only one big image of 2517 x 2335 pixels. We cropped 4 image crops of 256 x 256 pixels for test and use the rest for training. For the auxiliary RGBI SR task, we adopt the DIV2K Dataset [2]. Because the resolution of DIV2K is much higher than our HSIs, we first downsample them by a factor of x2 and take these downsampled images as our HR RGB images. After cropping, it leads to 137, 430 image patches of 64 x 64 pixels. This is about 34, 10, 6, and 40 times larger than CAVE, Harvard NTIRE, and Chikusei datasets, respectively.

Methods. We compare the proposed method to four state-of-the-art HSI SR methods: GDRRN [35], 3DFCNN [38], SSPSR [26], and MCNet [34]. We use the same training data for all methods and use the default training settings given by the authors of these methods. Bicubic interpola-

#(Mini-Batches)	0	1	2	3	4	5	6	8	10
RMSE ↓	0.01451	0.01357	0.01329	0.01309	0.01308	0.01305	0.01315	0.01315	0.01317

Table 1: Performance as a function of the number of mini-batches for RGBI SR loss.

Methods	RMSE ↓	MPSNR ↑	ERGAS ↓
Spatial Mixup [57]	0.01308	41.47317	3.77823
Cutblur Mixup [53]	0.01309	41.63031	3.69937
Spectral Mixup	0.01281	41.81709	3.64961

Table 2: Ablation study for *Spectral Mixup*

M	3	5	8	12
RMSE ↓	0.01321	0.01326	0.01315	0.01332
Training time (h)	2:14:40	1:49:11	1:24:14	1:15:04

Table 3: Influence of group size M on the performance.

tion is also introduced as a baseline.

Evaluation Metrics. We follow the literature and evaluate the performance of all methods under six standard metrics. They are cross correlation (CC) [36], spectral angle mapper (SAM) [55], root mean squared error (RMSE), erreur relative globale adimensionnelle de synthese (ERGAS) [47], peak signal-to-noise ratio (PSNR), and structure similarity (SSIM) [62]. For PSNR and SSIM of the reconstructed HSIs, their mean values of all spectral bands are reported. CC, SAM, and ERGAS are widely used in HSI fusion task, while the other three are standard metrics for image restoration and RGBI SR. Due to space limit, for some experiments, we only report numbers of three metrics and include the rest into the supplementary material.

Parameters. In this work, we focus on scaling factor $\times 4$ and $\times 8$. We report the results of $\times 4$ in the main paper, and report the results of $\times 8$ in the supplementary material. For the case of $\times 4$, we crop the images into patches of 64×64 pixels without overlapping to collect the training data. For $\times 8$, we use patches of 128×128 pixels. Those patches are then downsampled via Bicubic interpolation to obtain the corresponding LR HSI patches. The choice of value for other parameters are studied in Sec. 4.2.

Training Details. We use ADAM optimizer [28] and train all variants of our method for 10 epoches. This is a small number compared to the ones used by comparison methods. For instance, GDRRN [35] trains for 30 epoches, 3DFCNN [38] trains for 200 epoches, SSPSR [26] for 40 epoches, and MCNet [34] for 200 epoches. We choose a small number in order to thoroughly evaluate all the variants of our method. We find that 10 epoches are sufficient to give good results for our method, and believe a larger number probably can further push the numbers up. The initial learning rate of all our methods is set to 10^{-4} and is

reduced by a factor of 0.3 after every 3 epoches. As to the batch size, 16 is used for all experiments except for the case when the SSL loss is added. For that 8 is used due to the limit of GPU memory.

4.2. Ablation Study

We analyze the parameter choices of our method in this section. Experiments are conducted on the CAVE dataset in the semi-supervised setting.

Number of mini-batches. The number of mini-batches for labeled HSIs in each iteration is fixed to 1. The number of mini-batches for unlabeled HSIs for the SSL is fixed to 3. This is decided by the ratio of the size of unlabeled data to the size of labeled data. We have studied the influence of the other two parameters. First, for RGB data, we evaluate over a large range of values. The results are shown in Table 1. The performance increases first with the number of mini-batches and then decreases with it. We fix the number of batches for RGB data to 3 as it is a good trade-off between performance and computational time. We have also tested the number of mini-batches for the virtual samples created by *Spectral Mixup* and find that 2 is better than 1 and values larger than 2 add marginal improvement. We use 2 for all our experiments.

Influence of α . We tested five values for it: 0, 0.25, 0.5, 0.75 and 1 and obtained the following RMSE results: 0.01175 0.01178, 0.01173, 0.01187, and 0.01189. Results show that α should not be too big or too small. We choose $\alpha = 0.5$ to keep a balance between increasing data variation and preserving the fidelity of real HSIs.

Mixup Methods. We compare our *Spectral Mixup* to two recent data augmentation methods *mixup* [57] and *CutblurMixup* [53]. These methods also rely on the data mixing idea. Note that the results for this experiment are generated under a joint training with the auxiliary RGBI SR module as this is a stronger method than our base model. The results in Table 2 show that *Spectral Mixup* outperforms both of the methods. The spatial mixing method [57] blends data from two images. It may break detailed structures that are important for SR tasks. The *CutblurMixup* method learns *where to perform the SR* and is found helpful for RGB SR [53]. *Spectral Mixup* creates virtual examples by using convex combinations of spectral bands of the same image which avoids breaking image structures and preserves simple linear behavior in-between spectral bands. This makes it more suitable for HSI tasks.

Group Size. We evaluated four values for M . The re-

Methods	Components			CAVE			Harvard			NTIRE		
	RGBSR	<i>SMixup</i>	SSL	RMSE ↓	MPSNR ↑	ERGAS ↓	RMSE ↓	MPSNR ↑	ERGAS ↓	RMSE ↓	MPSNR ↑	ERGAS ↓
Ours				0.01451	40.83762	4.03386	0.01406	40.46614	3.17093	0.01602	38.31542	2.20746
Ours	✓			0.01309	41.64471	3.70784	0.01372	40.70069	3.09505	0.01519	38.78698	2.10917
Ours		✓		0.01353	41.51967	3.78138	0.01392	40.54614	3.13421	0.01563	38.58965	2.14927
Ours	✓	✓		0.01281	41.81709	3.64961	0.01359	40.75872	3.07788	0.01526	38.72326	2.11944
Ours	✓		✓	0.01254	42.01961	3.58921	0.01345	40.80595	3.06239	0.01509	38.83281	2.09676
Ours (final)	✓	✓	✓	0.01191	42.35848	3.44471	0.01331	40.93154	3.01392	0.01486	38.96572	2.06742
Bicubic	-	-	-	0.01856	38.73800	5.27190	0.01678	38.89758	3.80698	0.02353	34.74012	3.19014
GDRRN [35]	-	-	-	0.02463	36.27752	7.00438	0.01609	38.69532	4.30316	0.01974	36.07933	2.81752
3DFCNN [38]	-	-	-	0.01738	38.39284	6.70559	0.01578	39.34414	3.61725	0.02083	35.66309	2.82461
SSPSR [26]	-	-	-	0.01448	40.91316	4.04064	0.01427	40.32095	3.22745	0.01636	38.07401	2.25393
MCNet [34]	-	-	-	0.01461	40.73858	4.16596	0.014682	40.18739	3.26059	0.01680	38.02486	2.28342

Table 4: Results of all methods on the CAVE, Harvard, and NTIRE datasets in the semi-supervised setting for the $\times 4$ case.

Methods	Components			Metrics					
	RGBI SR	<i>S. Mixup</i>	SSL	RMSE ↓	CC ↑	MPSNR ↑	MSSIM ↑	ERGAS ↓	SAM ↓
Ours				0.01230	0.94992	39.71319	0.93529	5.32514	2.58381
Ours	✓			0.01211	0.95161	39.86037	0.93691	5.22631	2.53569
Ours		✓		0.01216	0.95097	39.82008	0.93649	5.26244	2.56245
Ours	✓	✓		0.01215	0.95096	39.8338	0.93675	5.24407	2.59671
Ours	✓		✓	0.01219	0.95109	39.81107	0.93617	5.25279	2.56749
Ours (final)	✓	✓	✓	0.01181	0.95375	40.09431	0.94035	5.08513	2.49154

Table 5: Results of all methods on the Chikusei dataset in the semi-supervised setting for the $\times 4$ case.

sults in Table 3 show that the performance of the method is robust to different values of M . It can also be found that $M = 8$ gives the best result in terms of RMSE and computational time. We thus use 8 for all our experiments. This finding is in line with [26].

4.3. Main Results

We first present the results in the semi-supervised setting. The results of all competing methods and all variants of our method on the CAVE, Harvard, and NTIRE dataset are shown in Table 4. The results in this table and other results in supplemental material show that our method outperforms all other state-of-the-art methods significantly and consistently over all datasets and under all evaluation metrics. We would like to point out that our baseline model – our method without any of the three proposed contributions – is already a top-performing method and performs better than other comparing methods.

The good performance of our base model is mainly due to the use of deep group convolutional networks for this task. Our results reinforce the findings made in [26] that group convolutional networks are good at extracting the correlation between spectral bands without increasing the model size. The network of [38] is quite shallow, probably because 3D convolution based methods are computationally heavy in general. We believe that this is the reason why

their method does not give top results. When compared to the very recent method MCNet [34], our base model also performs better in almost all cases. This is especially interesting because MCNet is trained for 200 epoches while our method is trained only for 10 epoches.

The proposed contributions, namely training with the auxiliary task RGBI SR, data augmentation via *Spectral Mixup* and the semi-supervised learning method based on cross-model consistency, all contribute significantly to the final results. Out of the three, learning with the auxiliary task RGBI SR and *Spectral Mixup* can work on its own. The SSL component needs to be used together with the auxiliary task RGBI SR. The results show that our SSL method can provide further improvement on top of the auxiliary RGBI SR method, and when the three components are combined together, we get the best performance – better than using any subsets of the proposed contributions. These observations are also well supported by our results on Chikusei with 128 bands in Table 5.

When more supervision is given such as in the fully-supervised setting, all conclusions we drawn in the semi-supervised setting hold as shown in Table 6. The results show that the proposed components are very effective and can be applied to situations with varying amount of HR HSIs. We show visual results of our method and two competing methods in Fig. 3. The figure shows that our method

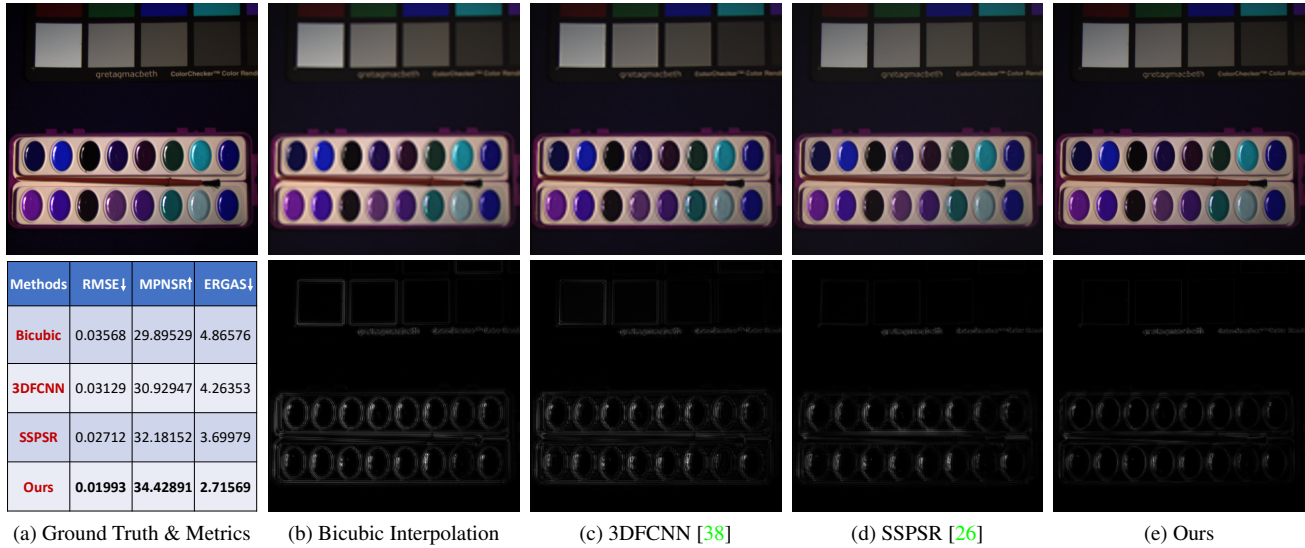


Figure 3: Exemplar results of our method and two competing methods trained in the semi-supervised setting on the CAVE dataset: top row for the super-resolved results and bottom row for the error maps.

Methods	Components		CAVE			Harvard		
	RGBI SR	<i>S. Mixup</i>	RMSE ↓	MPSNR ↑	ERGAS ↓	RMSE ↓	MPSNR ↑	ERGAS ↓
Ours			0.01196	42.38359	3.45903	0.01344	40.91014	3.01039
Ours	✓		0.01109	42.73668	3.35884	0.01325	41.03709	2.96643
Ours		✓	0.01134	42.88402	3.28051	0.01317	41.08568	2.95718
Ours	✓	✓	0.01068	43.32421	3.11799	0.01321	41.05925	2.96496
GDRRN [35]	-	-	0.01629	39.74705	4.52683	0.01484	39.62759	3.67932
3DFCNN [38]	-	-	0.01583	39.21786	5.41798	0.01519	39.66271	3.47738
SSPSR [26]	-	-	0.01245	42.13787	3.55146	0.01352	40.81499	3.05007
MCNet [34]	-	-	0.01245	42.25978	3.56246	0.01405	40.59229	3.10529

Table 6: Results of all methods on the CAVE and Harvard datasets in the fully-supervised setting for the $\times 4$ case.

generate few errors. More results can be found in the supplementary material.

4.4. Discussion

The superior performance shows that our method is able to learn from heterogeneous datasets and virtual examples rather than from purely HR HSIs. This greatly increases the amount of training data that can be used for HSI SR and can also include training samples for scenes such as moving objects that cannot be captured easily with the current hyperspectral imaging devices. We would like to point out that while the general concepts of learning with auxiliary tasks, data augmentation, and semi-supervised learning are well known, the challenge and novelty lie in defining proper auxiliary tasks for a new main task, proposing suitable augmentation technique and developing effective SSL methods for a new task. For instance, many seemingly-related auxil-

iary tasks yield no improvement or even degrade the performance of the main task [42]. -

5. Conclusion

In this paper, we have proposed a new method for hyperspectral image (HSI) super-resolution (SR). We build a deep group convolutional network which yields the state-of-the-art results. To further improve it, we have proposed three contributions. First, we extend the network such that the HSI SR task can be trained together with an auxiliary RGB image SR task to gain more supervision. Second, a simple, yet effective data augmentation method *Spectral Mixup* is proposed to create virtual training samples for HSI SR to increase the robustness of the network to new examples. Finally, the network is extended to also learn from datasets with LR HSIs only. The contributions greatly increase the amount of training data that HSI SR methods can

use. Extensive experiments show that all the three contributions are important and they help our method set a new state of the art on four public datasets.

References

- [1] H. K. Aggarwal and A. Majumdar. Hyperspectral image denoising using spatio-spectral total variation. *IEEE Geoscience and Remote Sensing Letters*, 13(3):442–446, 2016. 5
- [2] E. Agustsson and R. Timofte. Ntire 2017 challenge on single image super-resolution: Dataset and study. In *IEEE Conference on Computer Vision and Pattern Recognition Workshops (CVPRW)*, 2017. 5
- [3] T. Akgun, Y. Altunbasak, and R. M. Mersereau. Super-resolution reconstruction of hyperspectral images. *IEEE Transactions on Image Processing*, 14(11):1860–1875, 2005. 2
- [4] Naveed Akhtar, Faisal Shafait, and Ajmal Mian. Sparse spatio-spectral representation for hyperspectral image super-resolution. In *ECCV*, 2014. 2
- [5] N. Akhtar, F. Shafait, and A. Mian. Bayesian sparse representation for hyperspectral image super resolution. In *CVPR*, 2015. 2
- [6] Naveed Akhtar, Faisal Shafait, and Ajmal Mian. Hierarchical beta process with gaussian process prior for hyperspectral image super resolution. In Bastian Leibe, Jiri Matas, Nicu Sebe, and Max Welling, editors, *ECCV*, 2016. 2
- [7] Boaz Arad and Ohad Ben-Shahar. Sparse recovery of hyperspectral signal from natural rgb images. In *ECCV*, 2016. 2
- [8] Boaz Arad, Radu Timofte, Ohad Ben-Shahar, Yi-Tun Lin, and Graham D. Finlayson. Ntire 2020 challenge on spectral reconstruction from an rgb image. In *Proceedings of the IEEE/CVF Conference on Computer Vision and Pattern Recognition (CVPR) Workshops*, June 2020. 2, 5
- [9] Arun Balajee Vasudevan, Dengxin Dai, and Luc Van Gool. Semantic object prediction and spatial sound prediction with binaural sounds. In *European Conference on Computer Vision (ECCV)*, 2020. 2
- [10] Lucas Beyer, Xiaohua Zhai, Avital Oliver, and Alexander Kolesnikov. S4L: self-supervised semi-supervised learning. In *ICCV*, 2019. 2
- [11] J. M. Bioucas-Dias, A. Plaza, N. Dobigeon, M. Parente, Q. Du, P. Gader, and J. Chanussot. Hyperspectral unmixing overview: Geometrical, statistical, and sparse regression-based approaches. *IEEE Journal of Selected Topics in Applied Earth Observations and Remote Sensing*, 5(2):354–379, 2012. 2
- [12] A. Chakrabarti and T. Zickler. Statistics of Real-World Hyperspectral Images. In *CVPR*, 2011. 5
- [13] C. Chen, Y. Li, W. Liu, and J. Huang. Sirf: Simultaneous satellite image registration and fusion in a unified framework. *IEEE Transactions on Image Processing*, 24(11):4213–4224, 2015. 2
- [14] R. Cipolla, Y. Gal, and A. Kendall. Multi-task learning using uncertainty to weigh losses for scene geometry and semantics. In *CVPR*, 2018. 2
- [15] Dengxin Dai and Luc Van Gool. Ensemble projection for semi-supervised image classification. In *ICCV*, 2013. 2
- [16] R. Dian, L. Fang, and S. Li. Hyperspectral image super-resolution via non-local sparse tensor factorization. In *CVPR*, pages 3862–3871, 2017. 2
- [17] C. Dong, C. C. Loy, K. He, and X. Tang. Image super-resolution using deep convolutional networks. *IEEE Transactions on Pattern Analysis and Machine Intelligence*, 38(2):295–307, 2016. 2
- [18] W. Dong, F. Fu, G. Shi, X. Cao, J. Wu, G. Li, and X. Li. Hyperspectral image super-resolution via non-negative structured sparse representation. *IEEE Transactions on Image Processing*, 25(5):2337–2352, 2016. 2
- [19] Y. Fu, T. Zhang, Y. Zheng, D. Zhang, and H. Huang. Hyperspectral image super-resolution with optimized rgb guidance. In *CVPR*, 2019. 5
- [20] S. Galliani, Charis Lanaras, D. Marmanis, E. Baltsavias, and K. Schindler. Learned spectral super-resolution. *ArXiv*, abs/1703.09470, 2017. 2
- [21] Alexander F.H. Goetz. Three decades of hyperspectral remote sensing of the earth: A personal view. *Remote Sensing of Environment*, 113:S5 – S16, 2009. 1
- [22] A.A. Gowen, C.P. O’Donnell, P.J. Cullen, G. Downey, and J.M. Frias. Hyperspectral imaging – an emerging process analytical tool for food quality and safety control. *Trends in Food Science & Technology*, 18(12):590 – 598, 2007. 1
- [23] Yong Guo, Jian Chen, Jingdong Wang, Qi Chen, Jie Zhang Cao, Zeshuai Deng, Yanwu Xu, and Minghui Tan. Closed-loop matters: Dual regression networks for single image super-resolution. In *CVPR*, 2020. 2
- [24] Lukas Hoyer, Dengxin Dai, Yuhua Chen, Adrian Köring, Suman Saha, and Luc Van Gool. Three ways to improve semantic segmentation with self-supervised depth estimation. *arXiv preprint arXiv:2012.10782*, 2020. 2
- [25] J. Jiang, D. Liu, J. Gu, and S. Süsstrunk. What is the space of spectral sensitivity functions for digital color cameras? In *2013 IEEE Workshop on Applications of Computer Vision (WACV)*, 2013. 5
- [26] J. Jiang, H. Sun, X. Liu, and J. Ma. Learning spatial-spectral prior for super-resolution of hyperspectral imagery. *IEEE Transactions on Computational Imaging*, 6:1082–1096, 2020. 2, 3, 4, 5, 6, 7, 8, 12, 13, 14, 15, 16
- [27] J. Kim, J. K. Lee, and K. M. Lee. Accurate image super-resolution using very deep convolutional networks. In *CVPR*, 2016. 2
- [28] Diederik P. Kingma and Jimmy Ba. Adam: A method for stochastic optimization. In *ICLR*, 2015. 6
- [29] Durk P Kingma, Shakir Mohamed, Danilo Jimenez Rezende, and Max Welling. Semi-supervised learning with deep generative models. In *NeurIPS*. 2014. 2
- [30] W. Lai, J. Huang, N. Ahuja, and M. Yang. Deep laplacian pyramid networks for fast and accurate super-resolution. In *CVPR*, 2017. 2, 3
- [31] Samuli Laine and Timo Aila. Temporal ensembling for semi-supervised learning. In *ICLR*, 2017. 2
- [32] C. Lanaras, E. Baltsavias, and K. Schindler. Hyperspectral super-resolution by coupled spectral unmixing. In *2015*

- IEEE International Conference on Computer Vision (ICCV)*, 2015. 2
- [33] Christian Ledig, Lucas Theis, Ferenc Huszar, Jose Caballero, Andrew Cunningham, Alejandro Acosta, Andrew Aitken, Alykhan Tejani, Johannes Totz, Zehan Wang, and Wenzhe Shi. Photo-realistic single image super-resolution using a generative adversarial network. In *CVPR*, 2017. 2
- [34] Qiang Li, Qi Wang, and Xuelong Li. Mixed 2d/3d convolutional network for hyperspectral image super-resolution. *Remote Sensing*, 12(10), 2020. 2, 5, 6, 7, 8, 12, 13, 14, 15, 16
- [35] Y. Li, Lei Zhang, C. Ding, Wei Wei, and Y. Zhang. Single hyperspectral image super-resolution with grouped deep recursive residual network. *2018 IEEE Fourth International Conference on Multimedia Big Data (BigMM)*, 2018. 2, 5, 6, 7, 8, 12, 13, 14, 15, 16
- [36] L. Loncan, L. B. de Almeida, J. M. Bioucas-Dias, X. Briottet, J. Chanussot, N. Dobigeon, S. Fabre, W. Liao, G. A. Licciardi, M. Simões, J. Tourneret, M. A. Veganzones, G. Vivone, Q. Wei, and N. Yokoya. Hyperspectral pansharpening: A review. *IEEE Geoscience and Remote Sensing Magazine*, 3(3):27–46, 2015. 6
- [37] Guolan Lua and Baowei Fei. Medical hyperspectral imaging: a review. *Journal of Biomedical Optics*, 2014. 1
- [38] Shaohui Mei, Xin Yuan, Jingyu Ji, Yifan Zhang, Shuai Wan, and Qian Du. Hyperspectral image spatial super-resolution via 3d full convolutional neural network. *Remote Sensing*, 9(11), 2017. 2, 5, 6, 7, 8, 12, 13, 14, 15, 16
- [39] N. M. Nasrabadi. Hyperspectral target detection : An overview of current and future challenges. *IEEE Signal Processing Magazine*, 31(1):34–44, 2014. 1
- [40] Rang M. H. Nguyen, Dilip K. Prasad, and Michael S. Brown. Training-based spectral reconstruction from a single rgb image. In *ECCV*, 2014. 2
- [41] Ying Qu, Hairong Qi, and Chiman Kwan. Unsupervised sparse dirichlet-net for hyperspectral image super-resolution. In *CVPR*, 2018. 2
- [42] Baifeng Shi, Judy Hoffman, Kate Saenko, Trevor Darrell, and Huijuan Xu. Auxiliary task reweighting for minimum-data learning. In *NeurIPS*, 2020. 2, 8
- [43] W. Shi, J. Caballero, F. Huszár, J. Totz, A. P. Aitken, R. Bishop, D. Rueckert, and Z. Wang. Real-time single image and video super-resolution using an efficient sub-pixel convolutional neural network. In *CVPR*, 2016. 4
- [44] Z. Shi, C. Chen, Z. Xiong, D. Liu, and F. Wu. Hscnn+: Advanced cnn-based hyperspectral recovery from rgb images. In *IEEE/CVF Conference on Computer Vision and Pattern Recognition Workshops (CVPRW)*, 2018. 2
- [45] Antti Tarvainen and Harri Valpola. Mean teachers are better role models: Weight-averaged consistency targets improve semi-supervised deep learning results. 2017. 2
- [46] Simon Vandenhende, Stamatios Georgoulis, Marc Proesmans, Dengxin Dai, , and Luc Van Gool. Multi-task learning for dense prediction tasks: A survey, 2020. 2
- [47] L. Wald. Data fusion: definitions and architectures: fusion of images of different spatial resolutions. In *Presses des MINES*, 2002. 6
- [48] Qizhe Xie, Minh-Thang Luong, Eduard Hovy, and Quoc V. Le. Self-training with noisy student improves imagenet classification. In *CVPR*, 2020. 2
- [49] Qi Xie, Minghao Zhou, Qian Zhao, Deyu Meng, Wangmeng Zuo, and Zongben Xu. Multispectral and hyperspectral image fusion by MS/HS fusion net. In *CVPR*, 2019. 2
- [50] F. Yasuma, T. Mitsunaga, D. Iso, and S. K. Nayar. Generalized assorted pixel camera: Postcapture control of resolution, dynamic range, and spectrum. *IEEE Transactions on Image Processing*, 19(9):2241–2253, 2010. 5
- [51] N. Yokoya, C. Grohnfeldt, and J. Chanussot. Hyperspectral and multispectral data fusion: A comparative review of the recent literature. *IEEE Geoscience and Remote Sensing Magazine*, 5(2):29–56, 2017. 2
- [52] N. Yokoya and A. Iwasaki. Airborne hyperspectral data over chikusei. *Space Application Laboratory, University of Tokyo, Japan, Tech. Rep. SAL-2016-05-27*, May 2016. 5
- [53] Jaejun Yoo, Namhyuk Ahn, and Kyung-Ah Sohn. Rethinking data augmentation for image super-resolution: A comprehensive analysis and a new strategy. In *CVPR*, 2020. 4, 6
- [54] Y. Yuan, X. Zheng, and X. Lu. Hyperspectral image super-resolution by transfer learning. *IEEE Journal of Selected Topics in Applied Earth Observations and Remote Sensing*, 10(5):1963–1974, 2017. 2
- [55] R. H. Yuhas, A. F. Goetz, and booktitle=JPL, Summaries of the Third Annual JPL Airborne Geoscience Workshop year = 1992 J. W. Boardman, title=Discrimination among semi-arid landscape endmembers using the spectral angle mapper (sam) algorithm. 6
- [56] Amir Zamir, Alexander Sax, Teresa Yeo, Oğuzhan Kar, Nikhil Cheerla, Rohan Suri, Zhangjie Cao, Jitendra Malik, and Leonidas Guibas. Robust learning through cross-task consistency. In *CVPR*. 2020. 2
- [57] Hongyi Zhang, Moustapha Cisse, Yann N. Dauphin, and David Lopez-Paz. mixup: Beyond empirical risk minimization. In *International Conference on Learning Representations*, 2018. 4, 6
- [58] Lei Zhang, Jiangtao Nie, Wei Wei, Yanning Zhang, Shengcai Liao, and Ling Shao. Unsupervised adaptation learning for hyperspectral imagery super-resolution. In *CVPR*, 2020. 2
- [59] Yulun Zhang, Yapeng Tian, Yu Kong, Bineng Zhong, and Yun Fu. Residual dense network for image super-resolution. 2
- [60] Y. Zhao, Jinxiang Yang, Qingyong Zhang, L. Song, Y. Cheng, and Q. Pan. Hyperspectral imagery super-resolution by sparse representation and spectral regularization. *EURASIP Journal on Advances in Signal Processing*, 2011:1–10, 2011. 2
- [61] Y. Zhou, A. Rangarajan, and P. D. Gader. An integrated approach to registration and fusion of hyperspectral and multispectral images. *IEEE Transactions on Geoscience and Remote Sensing*, 58(5):3020–3033, 2020. 2
- [62] Zhou Wang, A. C. Bovik, H. R. Sheikh, and E. P. Simoncelli. Image quality assessment: from error visibility to structural similarity. *IEEE Transactions on Image Processing*, 13(4):600–612, 2004. 6

6. Supplementary Material

6.1. Further results for scaling factor $\times 4$

Due to space limitation, only results under three metrics, *i.e.*, RMSE, MPSNR, and ERGAS, are reported in the main paper. Here, we report the results under all six considered metrics, *i.e.*, RMSE, CC, MPSNR, MSSIM, ERGAS, and SAM. For the case of scaling factor $\times 4$ and in the semi-supervised setting, the results on the CAVE dataset, the Harvard dataset, the NTIRE2020 dataset are shown in Table 7, Table 8 and Table 9, respectively. The results under the full-supervision setting on the CAVE dataset and on the Harvard dataset are reported in Table 10 and Table 11¹.

These tables show that our method outperforms other comparison methods by a large margin under all six metrics. All our three contributions are useful and their combination yields the best results. The conclusions we have in the main paper hold for all the six metrics.

6.2. Results for scaling factor $\times 8$

We also provide results for scaling factor $\times 8$. The results on the CAVE, the Harvard, and the NTIRE2020 datasets in the semi-supervised setting are shown in Table 12, Table 13, and Table 14, respectively. It is evident from these tables that our method also outperforms other methods significantly and consistently for scaling factor $\times 8$. The same trend is observed for both $\times 4$ and $\times 8$ that all our three contributions are useful and their combination yields the best results. This demonstrates the applicability of our method across different scaling factors.

6.3. More visual results

We also provide more visual results on the NTIRE2020 datasets. For visualization, we use the same method as in the main paper. More specifically, we sample the 5th band, the 15th band and the 25th band of the hyperspectral image and assemble them together as an RGB image for visualization. The results of all methods on two different images for scaling factor $\times 8$ are provided in Fig. 4 and Fig. 5. To facilitate the comparison, we also show the error maps of all methods. The values in the error maps are the L2 distance between the predicted pixel values and the ground-truth pixel values, averaged over the three bands. It is clear from the visual results that our method generates better results than other methods. For instance, it produces sharper boundaries and less artefact.

¹The results on the NTIRE2020 dataset have not completed before the deadline unfortunately, but the obtained results show that the variants of our method with only a subset of our contributions already outperform all the competing methods.

Methods	Components			Metrics					
	RGB_SR	<i>Spec Mixup</i>	SSL	RMSE ↓	CC ↑	MPSNR ↑	MSSIM ↑	ERGAS ↓	SAM ↓
Ours				0.01451	0.99158	40.83762	0.95924	4.03386	4.16312
Ours	✓			0.01309	0.99282	41.64471	0.96379	3.70783	4.04210
Ours		✓		0.01353	0.99237	41.51967	0.96175	3.78138	3.75827
Ours	✓	✓		0.01253	0.99309	42.01961	0.96479	3.58920	3.73269
Ours	✓		✓	0.01281	0.99296	41.81709	0.96483	3.64962	3.88154
Ours (final)	✓	✓	✓	0.011909	0.99354	42.35848	0.96679	3.44471	3.78471
BicubicInt.	-	-	-	0.01856	0.98682	38.73800	0.94197	5.27190	4.17591
GDRRN [35]	-	-	-	0.02462	0.97819	36.27752	0.90681	7.00437	8.77122
3DFCNN [38]	-	-	-	0.01738	0.98182	38.39284	0.94719	6.70559	6.93475
SSPSR [26]	-	-	-	0.01448	0.99152	40.91316	0.95769	4.04064	4.07571
MCNet [34]	-	-	-	0.01461	0.99046	40.73858	0.95691	4.16595	4.59995

Table 7: Results of our method and other comparison methods on the CAVE dataset in the semi-supervised setting for the $\times 4$ case.

Methods	Components			Metrics					
	RGB_SR	<i>Spec Mixup</i>	SSL	RMSE ↓	CC ↑	MPSNR ↑	MSSIM ↑	ERGAS ↓	SAM ↓
Ours				0.014064	0.95902	40.46614	0.92537	3.17093	2.55144
Ours	✓			0.01371	0.95985	40.70068	0.92700	3.09505	2.54837
Ours		✓		0.01375	0.95951	40.63699	0.92726	3.12395	2.54555
Ours	✓	✓		0.01345	0.96077	40.80595	0.92896	3.06239	2.53140
Ours	✓		✓	0.01359	0.96003	40.75872	0.92855	3.07786	2.54378
Ours (final)	✓	✓	✓	0.01331	0.96111	40.93154	0.93004	3.01392	2.52215
BicubicInt.	-	-	-	0.01678	0.94994	38.89758	0.90925	3.80698	2.61754
GDRRN [35]	-	-	-	0.01609	0.94356	38.69531	0.91265	4.30316	3.05361
3DFCNN [38]	-	-	-	0.01578	0.95213	39.34413	0.91655	3.61724	2.72764
SSPSR [26]	-	-	-	0.01427	0.95818	40.32095	0.92356	3.22745	2.55649
MCNet [34]	-	-	-	0.01468	0.95779	40.18739	0.92140	3.26059	2.67236

Table 8: Results of our method and other comparison methods on the Harvard dataset in the semi-supervised setting for the $\times 4$ case.

Methods	Components			Metrics					
	RGB_SR	<i>Spec Mixup</i>	SSL	RMSE ↓	CC ↑	MPSNR ↑	MSSIM ↑	ERGAS ↓	SAM ↓
Ours				0.01602	0.99114	38.31541	0.93878	2.20746	1.14009
Ours	✓			0.01518	0.99198	38.78697	0.94278	2.10917	1.14217
Ours		✓		0.01563	0.99156	38.58965	0.94044	2.14927	1.14638
Ours	✓	✓		0.01509	0.99202	38.83281	0.94287	2.09676	1.13495
Ours	✓		✓	0.01526	0.99194	38.72326	0.94269	2.11944	1.13183
Ours (final)	✓	✓	✓	0.01485	0.99226	38.96572	0.94413	2.06742	1.12279
BicubicInt.	-	-	-	0.02353	0.98297	34.74012	0.90050	3.19014	3.89655
GDRRN [35]	-	-	-	0.01973	0.98578	36.07932	0.91738	2.81751	2.19765
3DFCNN [38]	-	-	-	0.02083	0.98732	35.66309	0.91799	2.82460	1.69877
SSPSR [26]	-	-	-	0.01635	0.99078	38.07401	0.93691	2.25392	1.43442
MCNet [34]	-	-	-	0.01680	0.99051	38.02486	0.93599	2.28342	1.45320

Table 9: Results of our method and other comparison methods on the NTIRE2020 dataset in the semi-supervised setting for the $\times 4$ case.

Methods	Components		Metrics					
	RGB_SR	<i>Spec Mixup</i>	RMSE ↓	CC ↑	MPSNR ↑	MSSIM ↑	ERGAS ↓	SAM ↓
Ours			0.01196	0.99350	42.38359	0.96631	3.45903	4.00592
Ours	✓		0.01109	0.99422	42.73668	0.96869	3.35884	4.17068
Ours		✓	0.01134	0.99397	42.88402	0.96798	3.28051	3.47102
Ours (final)	✓	✓	0.01068	0.99447	43.32421	0.96980	3.11799	3.68885
GDRRN [35]	-	-	0.01629	0.98975	39.74705	0.94418	4.52683	5.39660
3DFCNN [38]	-	-	0.01583	0.98538	39.21786	0.95165	5.41798	6.49516
SSPSR [26]	-	-	0.01245	0.99317	42.13787	0.96457	3.55146	3.83398
MCNet [34]	-	-	0.01245	0.99283	42.25978	0.96465	3.56246	3.84976

Table 10: Results of our method and other comparison methods on the CAVE dataest in the fully supervised case for **the** $\times 4$ case.

Methods	Components		Metrics					
	RGB_SR	<i>Spec Mixup</i>	RMSE ↓	CC ↑	MPSNR ↑	MSSIM ↑	ERGAS ↓	SAM ↓
Ours			0.01344	0.96101	40.91014	0.92836	3.01039	2.50704
Ours	✓		0.01325	0.96165	41.03709	0.92949	2.96643	2.49562
Ours		✓	0.01317	0.96200	41.08568	0.93056	2.95718	2.49771
Ours (final)	✓	✓	0.01321	0.96178	41.05925	0.93016	2.96496	2.49897
GDRRN [35]	-	-	0.01484	0.95102	39.62759	0.92013	3.67932	2.78624
3DFCNN [38]	-	-	0.01519	0.95411	39.66271	0.91944	3.47738	2.63534
SSPSR [26]	-	-	0.01352	0.96059	40.81499	0.92806	3.05007	2.51185
MCNet [34]	-	-	0.01405	0.96009	40.59229	0.92658	3.10529	2.59147

Table 11: Results of our method and other comparison methods on the Harvard dataset in the fully supervised case for **the** $\times 4$ case.

Methods	Components			Metrics					
	RGB_SR	<i>Spec Mixup</i>	SSL	RMSE ↓	CC ↑	MPSNR ↑	MSSIM ↑	ERGAS ↓	SAM ↓
Ours				0.02459	0.97233	35.89888	0.90591	7.11644	7.50539
Ours	✓			0.02300	0.97545	36.50494	0.91358	6.62181	6.89221
Ours		✓		0.02339	0.97705	36.64775	0.91078	6.45075	6.40468
Ours	✓	✓		0.02209	0.97923	37.14066	0.91748	6.14668	6.24141
Ours	✓		✓	0.02237	0.97732	36.87625	0.91685	6.34934	6.31945
Ours (final)	✓	✓	✓	0.02154	0.97963	37.35599	0.92070	6.00466	5.62054
BicubicInt.	-	-	-	0.03042	0.96665	34.22211	0.87386	8.43509	5.89620
GDRRN [35]	-	-	-	0.03473	0.95693	32.93635	0.83473	9.85545	11.05589
3DFCNN [38]	-	-	-	0.02920	0.90523	32.90242	0.87942	16.72651	10.43919
SSPSR [26]	-	-	-	0.02485	0.97260	35.88966	0.89926	7.03941	7.33639
MCNet [34]	-	-	-	0.02802	0.95804	34.31165	0.88028	10.29851	7.68969

Table 12: Results of our method and other comparison methods on the CAVE dataset in the semi-supervised setting for **the** $\times 8$ case.

Methods	Components			Metrics					
	RGB_SR	<i>Spec Mixup</i>	SSL	RMSE ↓	CC ↑	MPSNR ↑	MSSIM ↑	ERGAS ↓	SAM ↓
Ours				0.02263	0.92668	36.65405	0.86476	4.85976	2.91037
Ours	✓			0.02127	0.93172	37.14154	0.87229	4.58089	2.88299
Ours		✓		0.02219	0.92789	36.85938	0.86725	4.76278	2.89283
Ours	✓	✓		0.02117	0.93241	37.18768	0.87294	4.55818	2.85549
Ours	✓		✓	0.02116	0.93218	37.21642	0.87269	4.55045	2.88124
Ours (final)	✓	✓	✓	0.02100	0.93450	37.35231	0.87345	4.54990	2.88230
BicubicInt.	-	-	-	0.02495	0.91446	35.74092	0.84966	5.47721	3.00931
GDRRN [35]	-	-	-	0.02389	0.91131	35.64417	0.85316	5.72871	3.41440
3DFCNN [38]	-	-	-	0.02379	0.91813	36.05515	0.85651	5.21924	3.09288
SSPSR [26]	-	-	-	0.02282	0.92266	36.45639	0.86174	4.99781	3.07039
MCNet [34]	-	-	-	0.02348	0.92343	36.39212	0.85940	5.05722	3.14259

Table 13: Results of our method and other comparison methods on the Harvard dataset in the semi-supervised setting for **the $\times 8$ case**.

Methods	Components			Metrics					
	RGB_SR	<i>Spec Mixup</i>	SSL	RMSE ↓	CC ↑	MPSNR ↑	MSSIM ↑	ERGAS ↓	SAM ↓
Ours				0.02969	0.97146	32.83078	0.84733	4.04429	1.88851
Ours	✓			0.02839	0.97343	33.23283	0.85401	3.89444	1.83394
Ours		✓		0.03004	0.97055	32.75617	0.84575	4.08821	1.90378
Ours	✓		✓	0.02800	0.97355	33.23400	0.85870	3.88999	1.83009
Ours	✓	✓		0.02809	0.97385	33.33009	0.85599	3.85485	1.79814
Ours (final)	✓	✓	✓	0.02799	0.97560	33.45620	0.86001	3.84456	1.76943
BicubicInt.	-	-	-	0.03961	0.95195	29.95891	0.78926	5.45947	5.24567
GDRRN [35]	-	-	-	0.03596	0.95545	30.67236	0.80217	5.12654	3.21549
3DFCNN [38]	-	-	-	0.38575	-0.57977	9.17534	-0.47680	61.62476	163.56878
SSPSR [26]	-	-	-	0.03268	0.96529	31.78969	0.82646	4.49521	2.25976
MCNet [34]	-	-	-	0.03276	0.96623	31.96291	0.82932	4.41695	2.38619

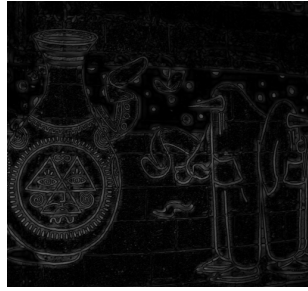
Table 14: Results of our method and other comparison methods on the NTIRE2020 dataset in the semi-supervised setting for **the $\times 8$ case**.



(a) Ground Truth



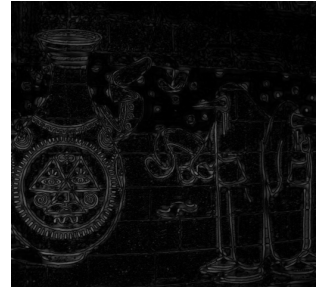
(b) Bicubic Interpolation



(c) Error of Bicubic



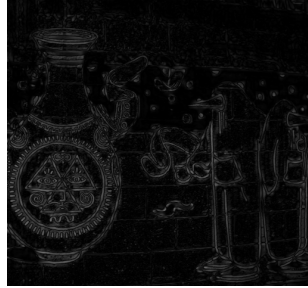
(d) GDRR [35]



(e) Error of GDRR



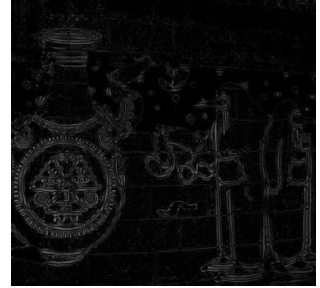
(f) 3DFCNN [38]



(g) Error of 3DFCNN



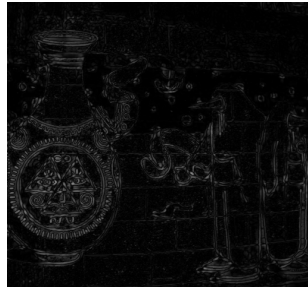
(h) SSISR [26]



(i) Error of SSISR



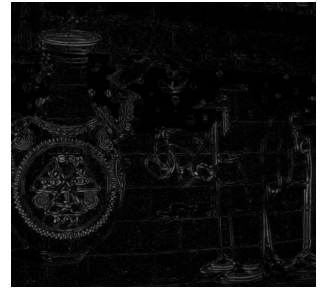
(j) MCNet [34]



(k) Error of MCNet



(l) Ours



(m) Error of Ours

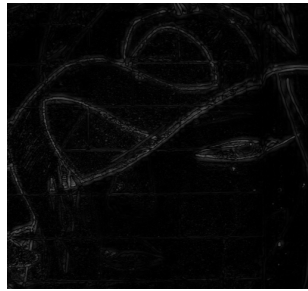
Figure 4: Exemplar results of $\times 8$ by our method and all comparison methods. The error is L2 distance to the ground-truth pixel values, averaged over the three bands.



(a) Ground Truth



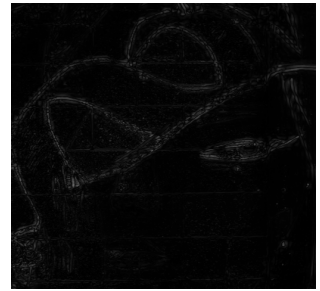
(b) Bicubic Interpolation



(c) Error of Bicubic



(d) GDRRN [35]



(e) Error of GDRRN



(f) 3DFCNN [38]



(g) Error of 3DFCNN



(h) SSPSR [26]



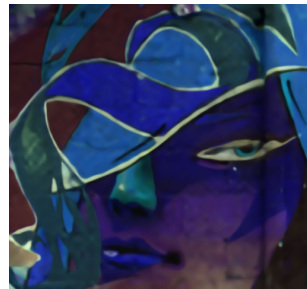
(i) Error of SSPSR



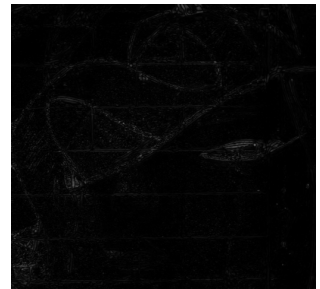
(j) MCNet [34]



(k) Error of MCNet



(l) Ours



(m) Error of Ours

Figure 5: Exemplar results of $\times 8$ by our method and all comparison methods. The error is L2 distance to the ground-truth pixel values, averaged over the three bands.